Negative Group Delay Phenomenon Analysis in Power Divider: Coupling Matrix Approach

Girdhari Chaudhary, *Member, IEEE*, and Yongchae Jeong, *Senior Member, IEEE*

***Abstract*— This paper presents a negative group delay (NGD) phenomenon analysis of a power divider using the coupling matrix approach. The proposed power divider can provide an arbitrary power division ratio with a minimal effect on group delay variations. From the analysis, it is found that the proposed circuit can provide positive group delay (PGD) and NGD through different transmission paths. The NGD can be generated without a lumped resistor and can be controlled by source-resonator coupling and unloaded-quality factor (Q_u) of resonators. For experimental validation, power dividers with PGD and NGD of 0.3 and −1 ns, respectively, were designed and fabricated. The measurement results agreed well with the simulation and the predicated values. The proposed power divider topology is useful for the performance improvement of microwave circuits and systems.**

***Index Terms*— Arbitrary power division ratio, coupling matrix, distributed topology, finite unloaded quality factor resonators, negative group delay (NGD), positive group delay (PGD).**

I. Introduction

POWER dividers have been widely adopted as basic building components in microwave circuits and systems [1]–[4]. Power dividers have been extensively studied over the past decades including the unequal and tunable power division ratio (k^2), circuit miniaturization, and multiband operation [1]–[9].

Because the group delay (GD) negatively influences the performance of RF/electronic circuits and systems, understanding effect of GD has become critical for communication systems. The GD is one of the bottlenecks in high-density electronic circuit development. However, GD analysis of power divider has rarely been considered in previous works, and the positive group delays (PGDs) have only been provided through different transmission paths [10].

The GD can be investigated by examining the frequency-dependent phase (φ) variation of the forward transmitting scattering parameter. Using the differential-phase GD (τ_g) relation

$$\tau_g = -\frac{d\varphi}{d\omega}. \tag{1}$$

The presence of negative group delay (NGD) is equivalent as an increasing phase (positive slope) with a frequency.

Modern RF wireless communication systems require highly linear high-power power amplifiers because of the complex modulation techniques that are needed to handle the higher data rate transmissions. A predistortion method is cost-effective linearization technique and has the advantages of low-power consumption and simple circuit configuration [11], [12]. In this technique, it is crucial to match GDs, the magnitudes, and phases of signals simultaneously in different paths to ensure linearity enhancement. For this purpose, a delay element, attenuator, and phase shifter were used in such circuits. Therefore, a power divider with predefined NGD would be promising for the PGD compensation in the predistortion amplifier that can eliminate the delay element and attenuator [12], [13].

The phased-antenna arrays suffer from a beam-squinting problem, which leads to an unwanted perturbation in direction and shape of the radiation pattern at a certain frequency. In [14] and [15], it is shown that the interelement GD of a feed network should have an abnormal GD, called NGD, for the beam-squint-free operation of the series-fed antenna arrays.

Various researchers have applied NGD circuits to design feed networks to minimize the beam-squint problems of the antenna arrays [14]–[18]. However, the conventional feed networks of antenna arrays designed using NGD circuits suffer from high insertion loss and small fractional bandwidths (FBWs). Also, in previous works, the NGD circuits and power dividers were designed independently, which required an additional interfacing matching network between them to integrate the conventional NGD circuit.

Similarly, the conventional NGD circuits suffer with narrow NGD bandwidth and magnitude (S_{21}) flatness [19]–[31]. While a few works have been performed for reducing signal attenuation (SA) [32]–[34], these works still suffer from small NGD bandwidth and the magnitude flatness problems. To overcome these problems, researchers have attempted to design NGD circuits using various methods such as cross-coupling between resonators [35], increasing the number of resonators [36], and transversal-filter topologies [37]. Moreover, except for the NGD proposed in [37], these NGD circuits also used lumped resistor R for generating NGD, which prevents fully distributed circuit realization.

Manuscript received November 8, 2016; revised January 6, 2017 and March 14, 2017; accepted April 19, 2017. Date of publication May 18, 2017; date of current version August 31, 2017. This work was supported in part by the Basic Science Research Program through the National Research Foundation of Korea (NRF) funded by the Ministry of Education, Science and Technology under Grant 2016R1D1A1A09918818 and in part by the Korean Research Fellowship Program through the NRF funded by the Ministry of Science, ICT and Future Planning under Grant 2016H1D3A1938065. Recommended for publication by Associate Editor A. Maffucci upon evaluation of reviewers' comments. *(Corresponding author: Yongchae Jeong.)*

The authors are with the Division of Electronic Engineering, IT Convergence Research Center, Chonbuk National University, Jeonju-si 54896, South Korea (e-mail: girdharic@jbnu.ac.kr; ycjeong@jbnu.ac.kr).

Color versions of one or more of the figures in this paper are available online at http://ieeexplore.ieee.org.

Digital Object Identifier 10.1109/TCPMT.2017.2696972

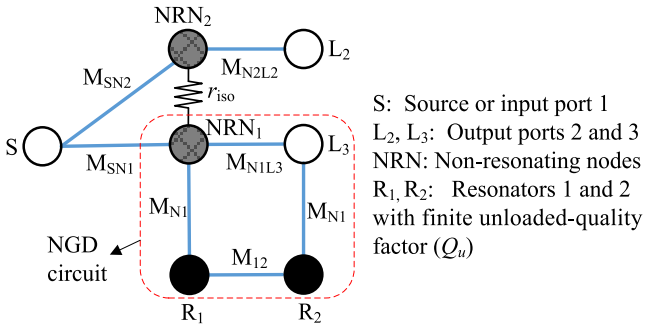

Fig. 1. Coupling diagram of the proposed power divider.

The coupling matrix method is widely used to design narrow filters with different functionalities such as tunable center frequency (f_0) and bandwidth, switchable filter from bandstop to all-pass filter, and the bandstop to bandpass switchable filter [38], [39]. Similarly, the coupling matrix approach is also applied to design filtering power dividers [40].

In this paper, the power divider with predefined GDs and arbitrary power division ratio along with the loss of NGD circuit is investigated based on the coupling matrix approach with the finite unloaded-quality factor (Q_u) of resonators. The proposed power divider provides PGD and NGD through different transmission paths. This work does not require a lumped resistor to generate NGD; otherwise, the NGD is controlled by input–output external couplings Q_u and inter-resonator couplings between resonators.

II. Mathematical Analysis

Fig. 1 shows the coupling diagram of the proposed power divider, where nodes R_1 and R_2 present the resonators with finite Q_u. Similarly, nodes S, NRN, and L represent the source, nonresonating node, and load, respectively. Therefore, S, L_2, and L_3 denote the input port 1, output port 2, and output port 3, respectively. Since the proposed structure is not symmetrical, the modified even- and odd-mode analysis can be applied to find the S-parameters of the proposed power divider. The general S-parameters of three-port power divider assuming the power division ratio of 1: k^2 are can be expressed in terms of the even- and odd-mode S-parameters of subcircuits as [41]

$$S_{11} = \frac{S_{11e}^{21} + S_{11e}^{31}}{2} = S_{11e}^{21} = S_{11e}^{31} \tag{2a}$$

$$S_{22} = \frac{k^2 S_{22e}^{21} + S_{22o}^{21}}{1+k^2} \quad S_{33} = \frac{k^2 S_{33e}^{31} + S_{33o}^{31}}{1+k^2} \tag{2b}$$

$$S_{21} = \frac{S_{21e}^{21}}{\sqrt{1+k^2}} \quad S_{31} = \frac{k S_{31e}^{31}}{\sqrt{1+k^2}} \tag{2c}$$

$$S_{23} = \frac{k\left(S_{22e}^{21} - S_{33o}^{31}\right)}{1+k^2} \tag{2d}$$

where symbols e and o correspond to the even- and odd-mode equivalent subcircuits, respectively. Here, S_{11e}^{21}, S_{22e}^{21}, S_{21e}^{21}, and S_{22o}^{21} represent even- and odd-mode S-parameters of the subcircuit between ports 2 and 1. Similarly, S_{11e}^{31}, S_{33e}^{31}, S_{31e}^{31}, and S_{33o}^{31} denote the even- and odd-mode S-parameters of subcircuit between ports 3 and 1.

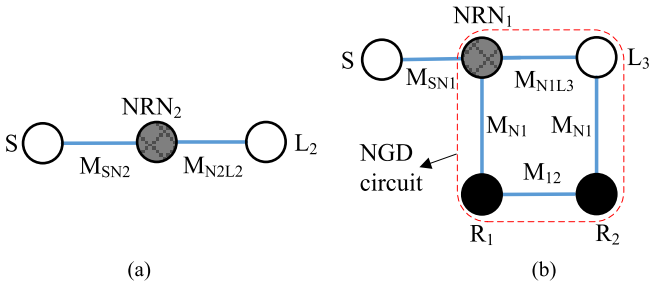

Fig. 2. Modified even-mode excitation equivalent coupling diagrams. (a) Between ports 2 and 1. (b) Between ports 3 and 1.

A. Even-Mode Analysis

Fig. 2(a) shows the equivalent even-mode coupling diagram between ports 2 and 1. In Fig. 2(a), M_{SN2} and M_{N2L2} show the coupling between S and NRN_2, and between L_2 and NRN_2, respectively. When the power division is assumed as 1:k^2, the equivalent normalized termination impedances of the source and load between ports 2 and 1 are expressed [7] as follows:

$$r_{Se}^{21} = 1 + k^2 \quad r_{L2e}^{21} = 1. \tag{3}$$

The coupling between the source/load and NRNs can allow a $\lambda/4$ transmission line such that the normalized characteristic impedance is equivalent to the inverse of coupling the coefficient. Using the equivalent even-mode coupling diagram between ports 2 and 1 shown in Fig. 2(a), the even-mode S-parameters of subcircuit can be found. For the matched input and output reflection conditions ($S_{11e}^{21} = S_{22e}^{21} = 0$) at f_0, the values of the normalized coupling between the source/load and NRN_2 are obtained as follows:

$$M_{SN2} = \frac{1}{k}\frac{1}{\sqrt{1+k^2}} \tag{4a}$$

$$M_{N2L2} = \frac{1}{k}. \tag{4b}$$

Furthermore, the transmission coefficient magnitude and associated GDs between ports 2 and 1 of the proposed power divider at f_0 are determined as (5) for matched input–output reflection coefficients

$$S_{21p}|_{f=f_0} = \left.\frac{S_{21e}^{21}}{\sqrt{1+k^2}}\right|_{f=f_0} = \frac{2\sqrt{r_{Se}^{21}} M_{N2L2} M_{SN2}}{\sqrt{1+k_1^2}\left(r_{Se}^{21} M_{SN2}^2 + M_{N2L2}^2\right)} = \frac{1}{\sqrt{1+k^2}} \tag{5a}$$

$$\tau_{21p}|_{f=f_0} = \frac{1+2k^2+\sqrt{(1+k^2)}+k^2\sqrt{(1+k^2)}}{8 f_0 \sqrt{k^2(1+k^2)}}. \tag{5b}$$

Fig. 2(b) shows the equivalent even-mode coupling diagram between ports 3 and 1. In this subcircuit, M_{SN1} represents the coupling between S and NRN_1. The normalized termination impedance between ports 3 and 1 can be expressed [7] as follows:

$$r_{Se}^{31} = (1+k^2)/k^2 \quad r_{L3e}^{31} = 1. \tag{6}$$

The normalized coupling M_{SN1} will transform normalized source impedance shown in (6) to normalized NRN_1 impedance that is equal to 1. Similarly, NRN_1, L_3, R_1, and R_2

form the second-order NGD filter, of which the $(N+2)\times(N+2)$ normalized coupling matrix is defined by

$$M_{\mathrm{NGD}} = \begin{bmatrix} 0 & M_{\mathrm{N1}} & 0 & M_{\mathrm{N1L3}} \\ M_{\mathrm{N1}} & \dfrac{-j}{Q_u\Delta} & M_{12} & 0 \\ 0 & M_{12} & \dfrac{-j}{Q_u\Delta} & M_{\mathrm{N1}} \\ M_{\mathrm{N1L3}} & 0 & M_{\mathrm{N1}} & 0 \end{bmatrix} \tag{7}$$

where the subscripts N1, L3, 1, and 2 are the NRN_1 as input port, output port 3, the first resonator, and the second resonator, respectively. Similarly, Δ is a 3-dB FBW. The normalized coupling M_{12} is assumed as aM_{N1}^2, where a is any positive number. Using equivalent even-mode subcircuit shown in Fig. 2(b), the coupling between source (S) and NRN_1 can be found as (8) for matching condition ($S_{11e}^{31}=0$) at f_0

$$M_{\mathrm{SN1}} = \frac{k}{\sqrt{1+k^2}}. \tag{8}$$

Similarly, the transmission coefficient magnitude between ports 3 and 1 of the proposed power divider at f_0 is calculated as (9) and (10) with matched input–output reflection coefficients

$$S_{31p}|_{f=f_0} = \left.\frac{kS_{31e}^{31}}{\sqrt{1+k^2}}\right|_{f=f_0} = \frac{k\times S_{\mathrm{S\text{-}N_1}}|_{f=f_0}\times S_{\mathrm{NGD}}|_{f=f_0}}{\sqrt{1+k^2}} \tag{9}$$

where

$$S_{\mathrm{S\text{-}N_1}}|_{f=f_0} = \frac{2\sqrt{r_{\mathrm{Se}}^{31}}M_{\mathrm{SN1}}}{\left(r_{\mathrm{Se}}^{31}M_{\mathrm{SN1}}^2+1\right)} = 1 \tag{10a}$$

$$S_{\mathrm{NGD}}|_{f=f_0} = \frac{2\left(\frac{M_{\mathrm{N1L3}}}{Q_u^2\Delta^2}+a^2M_{\mathrm{N1L3}}M_{\mathrm{N1}}^4-aM_{\mathrm{N1}}^4\right)}{\left\{\begin{array}{l}\left(M_{\mathrm{N1L3}}^2+1\right)\left(\frac{1}{Q_u^2\Delta^2}+a^2M_{\mathrm{N1}}^4\right)\\ +\frac{2M_{\mathrm{N1}}^2}{Q_u\Delta}+M_{\mathrm{N1}}^4(1-2aM_{\mathrm{N1L3}})\end{array}\right\}}. \tag{10b}$$

As seen from (9) and (10), the magnitude of transmission coefficient between ports 3 and 1 depends on the transmission coefficient magnitudes of source and NRN_1 and NGD circuit. Since the NGD occurs under SA condition, the insertion loss between paths 3 and 1 increases as compared to the conventional power dividers. Similarly, GD between ports 3 and 1 of the proposed power divider at f_0 is further simplified as

$$\begin{aligned}\tau_{31p}|_{f=f_0} &= \frac{1}{4f_0}\left\{\frac{1+2k^2}{2k\sqrt{1+k^2}} + \frac{8Q_uM_{\mathrm{N1L3}}}{\pi aM_{\mathrm{N1}}^4\left(1-aM_{\mathrm{N1L3}}\right)Q_u^2\Delta^2-\pi M_{\mathrm{N1L3}}}\right\} \\ &+ \frac{1}{\pi f_0}\left\{\frac{M_{\mathrm{N1}}^2Q_u^2\Delta+Q_uM_{\mathrm{N1L3}}^2+Q_u}{\left[\begin{array}{l}0.5\left(M_{\mathrm{N1L3}}^2+1\right)\left(1+Q_u^2\Delta^2a^2M_{\mathrm{N1}}^4\right)\\ +M_{\mathrm{N1}}^2Q_u\Delta-Q_u^2\Delta^2M_{\mathrm{N1}}^4(aM_{\mathrm{N1L3}}-0.5)\end{array}\right]}\right\}\end{aligned} \tag{11}$$

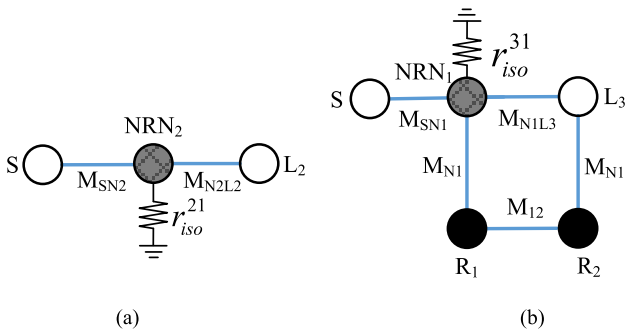

Fig. 3. Modified odd-mode excitation equivalent coupling diagrams. (a) Between ports 2 and 1. (b) Between ports 3 and 1.

where

$$M_{\mathrm{N1L3}} = \frac{aM_{\mathrm{N1}}^4 \mp \sqrt{a^2M_{\mathrm{N1}}^8+\left(a^2M_{\mathrm{N1}}^4+\frac{1}{Q_u^2\Delta^2}\right)\left\{M_{\mathrm{N1}}^4\left(a^2-1\right)+\frac{1}{Q_u^2\Delta^2}\right\}}}{a^2M_{\mathrm{N1}}^4+\frac{1}{Q_u^2\Delta^2}}. \tag{12}$$

In (12), the positive sign is used in the case of $M_{\mathrm{N1}}>0$ and the negative sign is used for $M_{\mathrm{N1}}<0$. As seen from (5b), the GD between paths 2 and 1 is always positive, whereas the GD between paths 3 and 1 is negative depending on the value of the coupling coefficient and Q_u of the resonators.

B. Odd-Mode Analysis

Fig. 3 shows the equivalent circuits under odd-mode excitation where normalized termination impedances of source between ports 2 and 1 (r_{So}^{21}) and ports 3 and 1 (r_{So}^{31}) are given as

$$r_{\mathrm{So}}^{21} = r_{\mathrm{So}}^{31} = 0. \tag{13}$$

Since the source impedances are short-circuited, no signal transmissions take place under odd-mode excitation. In addition, normalized isolation resistors under the odd-mode excitation are given as

$$r_{\mathrm{iso}}^{21} = k^2 \quad r_{\mathrm{iso}}^{31} = 1. \tag{14}$$

For simplicity, the termination impedance of NRN_2 and NRN_1 is assumed same as r_{iso}^{21} and r_{iso}^{31}, which is transformed to load impedance at ports 2 and 3 by M_{N2L2} and NGD circuit, respectively. Similarly, for the infinite isolation ($S_{23}=0$) between output ports, the value of the normalized isolation resistor (r_{iso}) can be found as

$$r_{\mathrm{iso}} = 1+k^2. \tag{15}$$

To illustrate the design equations of the proposed power divider, the synthesized results are shown in Fig. 4. To obtain GD of -1 ns at 2.14 GHz through ports 3 and 1, the calculated coupling matrix parameters of the proposed power divider are shown in Table I. As observed from the synthesized results shown in Fig. 4(a), the magnitudes of the transmission S-parameters changed with k^2. Moreover, as shown in Table I, the magnitude of S_{31} in the proposed power divider is higher

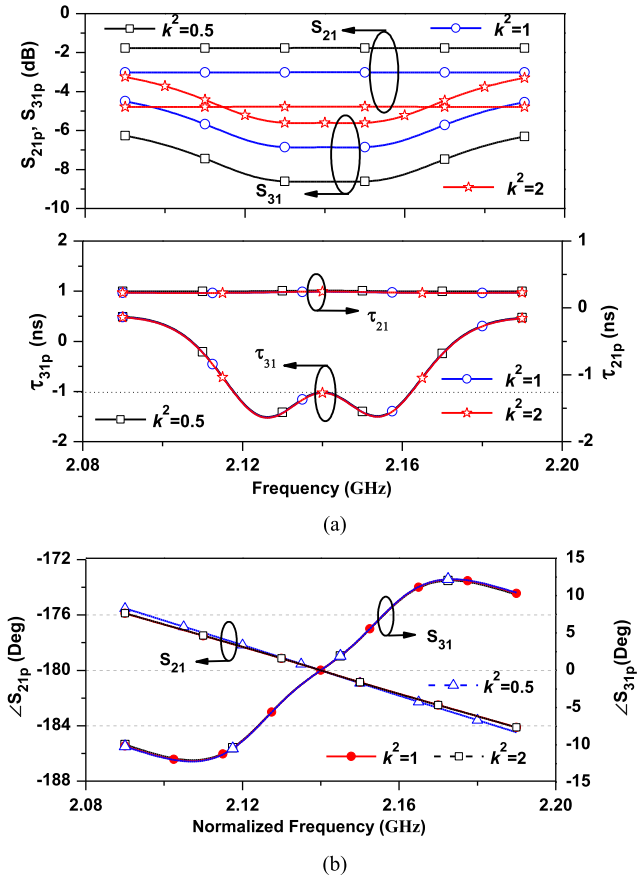

Fig. 4. Synthesized results of power divider with different k^2 and $Q_u = 50$, $\Delta = 2\%$, and $f_0 = 2.14$ GHz. (a) Magnitude/GD. (b) Phase characteristics.

TABLE I

CIRCUIT PARAMTERS AND S-PARAMETER MAGNITUDES FOR POWER DIVIDER WITH NGD $= -1$ ns WITH $Q_u = 50$ AND $\Delta = 2\%$

k^2	M_{SN1}	M_{SN2}	M_{N2L2}	M_{N1}	M_{N1L3}	a	r_{iso}	S_{31c}	S_{NGD}	S_{31p}
0.5	1.1547	0.5773	1.4142	0.7	-0.734	0.86	1.5	-4.77	-3.84	-8.61
1	0.7070	0.7070	1	0.7	-0.734	0.86	2	-3.01	-3.84	-6.85
2	0.4082	0.8165	1	0.7	-0.734	0.86	3	-1.76	-3.84	-5.60

S-paramter magntiudes at f_0
S_{31c}: conventional power divider, S_{31p}: proposed power divider,
$S_{21c} = S_{21p}$

than the conventional because the insertion loss of NGD circuit is added in this path as given in (9) and (10). However, the GDs of the different transmission paths (τ_{21} and τ_{31}) are almost constant and independent of k^2.

Fig. 4(b) shows the synthesized phase characteristics of the power divider. In this result, the phase slope of S_{21} is negative whereas the phase slope of S_{31} is positive and does not change with k^2. Similarly, Fig. 5 shows the synthesized input–output return losses (S_{ii}) and isolation (S_{23}) between the output ports for different k^2. As shown in Fig. 5, the input–output ports are matched and the infinite isolation (S_{23}) between output ports at the f_0 is obtained for all values of k^2.

To illustrate the effect of Q_u on the magnitudes of the transmission coefficients and GDs, the synthesized results are

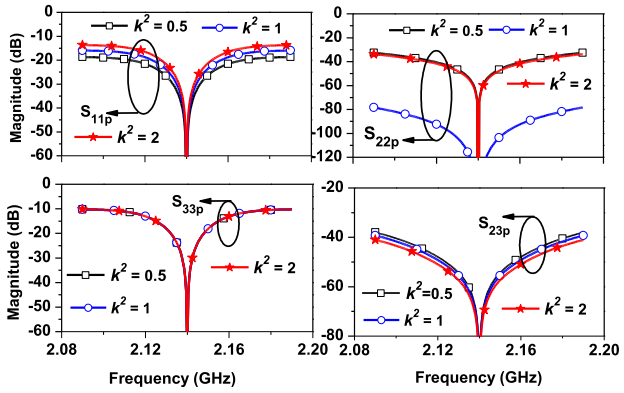

Fig. 5. Synthesized return loss/isolation characteristics of power divider with different k^2 and $Q_u = 50$, $\Delta = 2\%$, and $f_0 = 2.14$ GHz.

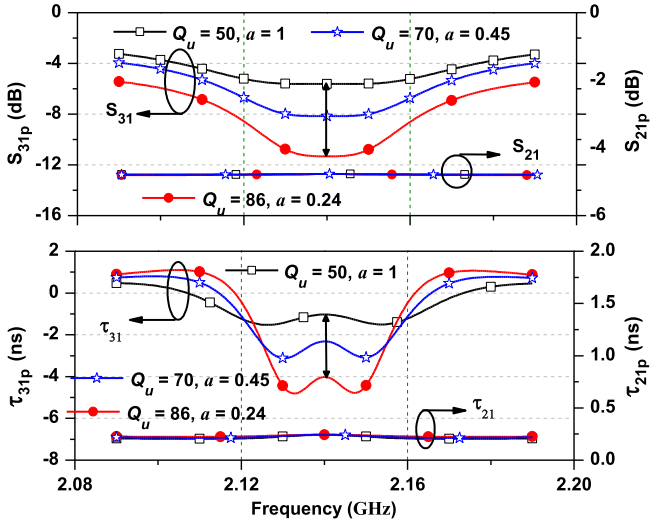

Fig. 6. Synthesized magnitude/GD results with $k^2 = 2$, $M_{N1} = 0.70$, $M_{12} = aM_{N1}^2$, and different values of Q_u.

shown in Fig. 6 for different Q_u. In this simulation, the circuit parameters are assumed as $f_0 = 2.14$ GHz, $k^2 = 2$, $M_{N1} = 0.70$, and $M_{12} = aM_{N1}^2$, and GD is maintained within $\tau_{31}|_{f_0} \pm 0.5$ ns. As observed in Fig. 6, the magnitude and GD of S_{31} decrease when Q_u changes from 50 to 86. As NGD increases, the NGD bandwidth (which is defined as bandwidth of GD < 0) slightly decreases. Therefore, a tradeoff occurs between NGD, the insertion loss, and the NGD bandwidth. However, the magnitude and GD of S_{21} are almost constant for every Q_u.

To illustrate the effect of Q_u, the calculated magnitude and GD of S_{31}, the NGD bandwidth, and the interresonator couplings are shown in Fig. 7 for different Q_u. In this calculation, the value of M_{N1} is assumed as 0.70 and 1.10. Similarly, the GD of S_{31} was maintained as $\tau_{31}|_{f_0} \pm 0.25$ ns. As shown in Fig. 7, the magnitude and GD of S_{31} increase and interresonator coupling coefficient decreases as the value of Q_u changes from 40 to 90. In addition, the NGD bandwidth decreases as GD increases. However, the NGD bandwidth is almost the same in both cases ($M_{N1} < 1$ and $M_{N1} > 1$).

Similarly, to investigate the effect of the coupling coefficient (M_{N1}) between NRN_1 and the resonator, the calculated

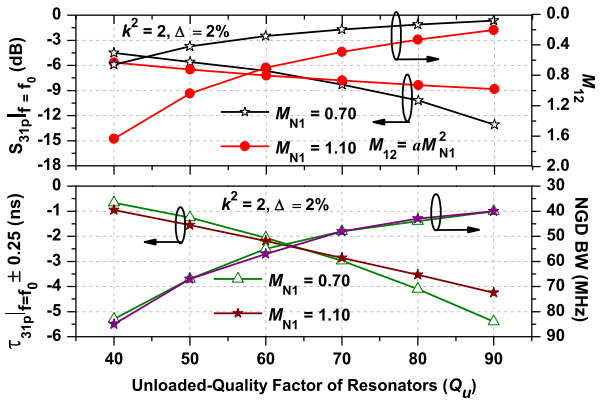

Fig. 7. Magnitude/GD and NGD bandwidth variations according to unloaded-quality factors.

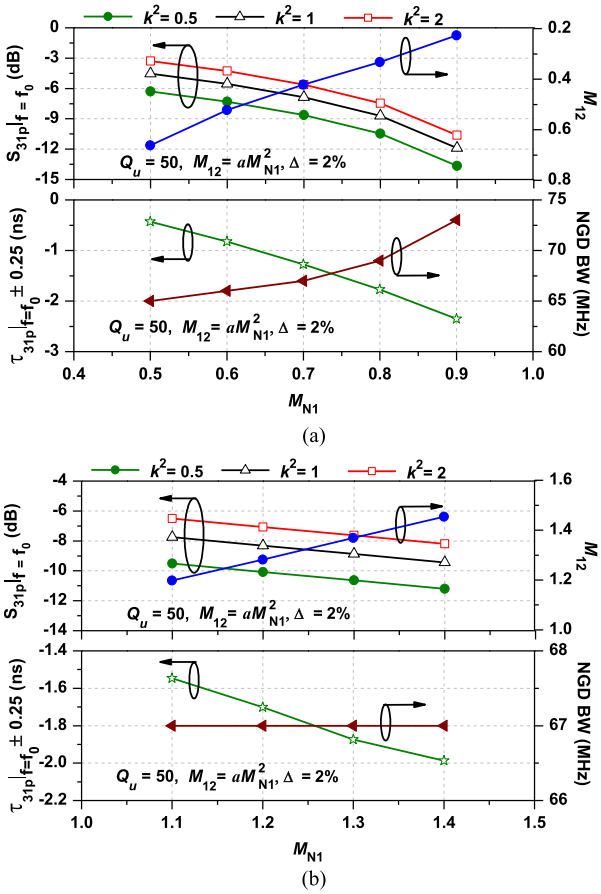

Fig. 8. Magnitude/GD and NGD bandwidth variations according to M_{N1}. (a) $M_{N1} < 1$. (b) $M_{N1} > 1$.

magnitude and GD of S_{31} and the coupling coefficient (M_{12}) between the resonators and the NGD bandwidth are shown in Fig. 8. When M_{N1} increases toward 0.9 as shown in Fig. 8(a), the NGD bandwidth changes from 65 to 74 MHz, but remains constant when $M_{N1} > 1$ as shown in Fig. 8(b). Similarly, M_{12} decreases in case of $M_{N1} < 1$ and increases in the case of $M_{N1} > 1$ when GD is provided a higher negative value. However, the magnitude of S_{31} in the condition of $M_{N1} < 1$ is smaller than in the condition of $M_{N1} > 1$. As observed from Figs. 6 and 7, it can be concluded that the NGD and bandwidth are independent of k^2 and fully dependent of the NGD circuit parameters such as M_{N1} and Q_u.

The design procedure for the proposed power dividers is summarized as follows.

1) Specify the center frequency f_0, power division ratio k^2, maximum achievable NGD, SA, Q_u, and Δ.
2) Calculate the values of M_{SN2}, M_{N2L2}, and M_{SN1} using (4) and (8).
3) Obtain value of M_{N1L3} using (12) by assuming the values of M_{N1} and a.
4) After obtaining the value of M_{N1L3}, calculate S_{31} and NGD using (9)–(11).
5) Compare the calculated achievable NGD (τ_{cal}) to the specified value (τ_{req}). If $|(\tau_{cal} - \tau_{req})| \leq 0.001$ ns, then M_{N1}, M_{N1L3}, and M_{12} are the correct values of the specified NGD. If this condition is not satisfied, then change M_{N1}, and repeat steps (3) and (4).
6) Implement the coupling between S-NRN$_2$ (M_{SN2}) NRN$_2$-L$_2$ (M_{N2L2}) and S-NRN$_1$ (M_{SN1}) by the $\lambda/4$ transmission line with normalized characteristic impedances of $1/M_{SN2}$, $1/M_{N2L2}$, and $1/M_{SN1}$, respectively. The characteristic impedances of transmission line can be renormalized by multiplying the values with reference port impedance Z_0.
7) After obtaining the normalized couplings (M_{N1}, M_{12}, and M_{N1L3}) of NGD circuit, calculate coupling coefficients k_{N1}, k_{12}, and k_{N1L3} using

$$k_{N1} = M_{N1}\sqrt{\Delta} = 1/\sqrt{Q_{exe}} \qquad k_{12} = M_{12}\Delta$$
$$k_{N1L3} = M_{N1L3}\Delta \tag{16}$$

where k_{N1} represents coupling coefficient between R$_1$-NRN$_1$ and R$_2$-L$_3$ of NGD circuit. Similarly, k_{12} and k_{N1L3} represent coupling coefficient between R$_1$-R$_2$ and NRN$_1$-L$_3$ of NGD circuit, respectively.
8) Implement k_{N1L3} with $3\lambda/4$ step impedance line with characteristic impedances Z_1 and Z_2. The relation between characteristic impedances and k_{N1L3} is given as (17). The extracted k_{N1L3} is shown in Fig. 9(a)

$$k_{N1L3} = \frac{Z_2}{Z_1^2}. \tag{17}$$

9) The interresonator (R_1-R_2) coupling coefficient k_{12} can be extracted by controlling length L_5 and gap g_2 as shown in Fig. 9(c). Similarly, Q_{exe} and k_{N1} can be extracted by controlling L_3 and g_1 as shown in Fig. 9(b) and (d).
10) Finally, optimize the physical dimensions of the power divider using a full-wave electromagnetic (EM) simulator.

III. Simulation and Measurement Results

For experimental demonstration purposes, power dividers with $k^2 = 0.6$, 1, and 2 were fabricated at f_0 of 2.14 GHz on FR4 epoxy substrate with a dielectric constant (ε_r) of 4.48, thickness (h) of 0.787 mm, and loss tangent of 0.02. The design goal was to obtain NGD of -1 ns at f_0 for each power divider. The physical dimensions of the fabricated circuits were optimized using ANSYS HFSS 15.

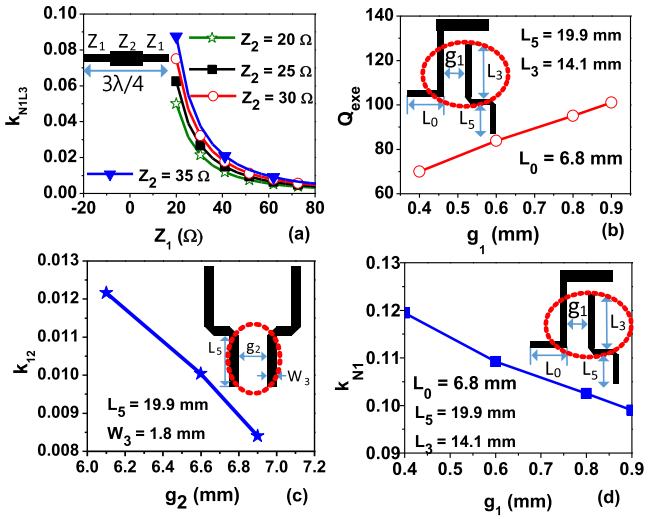

Fig. 9. Extracted parameters with FR4-epoxy substrate with $\varepsilon_r = 4.4$, $h = 0.787$ mm, and $\tan\delta = 0.02$. (a) Source-load (NRN_1-L_3) coupling coefficient k_{N1L3}. (b) External quality factor Q_{exe}. (c) Interresonator (R_1-R_2) coupling coefficient k_{12}. (d) Input–output (NRR_1-R_1 and R_2-L_3) coupling coefficients k_{N1}.

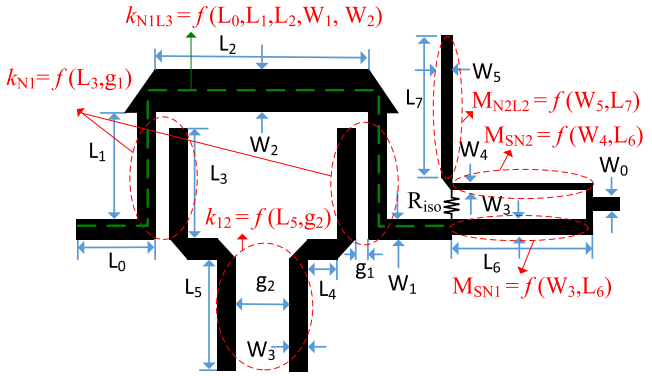

Fig. 10. EM-simulation layout of power divider with $k^2 = 0.6$. Physical dimensions: $L_0 = 16.8$, $L_1 = 12.2$, $L_2 = 18$, $L_3 = 14$, $L_4 = 1.5$, $L_5 = 20$, $L_6 = 19$, $L_7 = 19$, $W_0 = 1.5$, $W_1 = 1.8$, $W_2 = 3.70$, $W_3 = 0.98$, $W_4 = 0.34$, $W_5 = 1.02$, $g_1 = 0.5$, and $g_2 = 6.8$ (unit: mm).

Using the design method described above, the coupling parameters for the power divider with $k^2 = 0.6$ are calculated as $M_{SN2} = 1.0206$, $M_{N2L2} = 1.291$, $M_{SN1} = 0.6124$, $M_{N1} = 1.04$, $M_{12} = 1.1897$, $M_{N1L3} = 1.4269$, $Q_u = 50$, and $\Delta = 2\%$.

Fig. 10 shows the EM-simulation layout with the physical dimensions of the fabricated power divider. The simulated and measured magnitudes and GDs are shown in Fig. 11(a). From the measurement, the values of magnitudes and GDs are $S_{21} = -2.26$ dB, $S_{31} = -9.96$ dB, $\tau_{21} = 0.3204$ ns, and $\tau_{31} = -0.8656 \pm 0.08$ ns at $f_0 = 2.141$ GHz. The measured NGD bandwidth is given as 60 MHz. Similarly, Fig. 11(b) shows the simulated and measured return losses and isolation characteristics. The measured return losses and isolation are determined as $S_{11} = -21.97$ dB, $S_{22} = -18.98$ dB, $S_{33} = -17.93$ dB, and $S_{23} = -39.12$ dB at f_0. The return losses and isolation are higher than 11.1 dB and 33.4 dB, respectively, in the overall measured frequencies.

The calculated coupling parameters for the power divider with $k^2 = 1$ are given as $M_{SN2} = 0.7071$, $M_{N2L2} = 1$, $M_{SN1} = 0.7071$, $M_{N1} = 1.04$, $M_{12} = 1.1897$, $M_{N1L3} = 1.4269$, $Q_u = 50$, and $\Delta = 2\%$. The EM-simulation layout with physical dimensions is shown in Fig. 12 after the optimization.

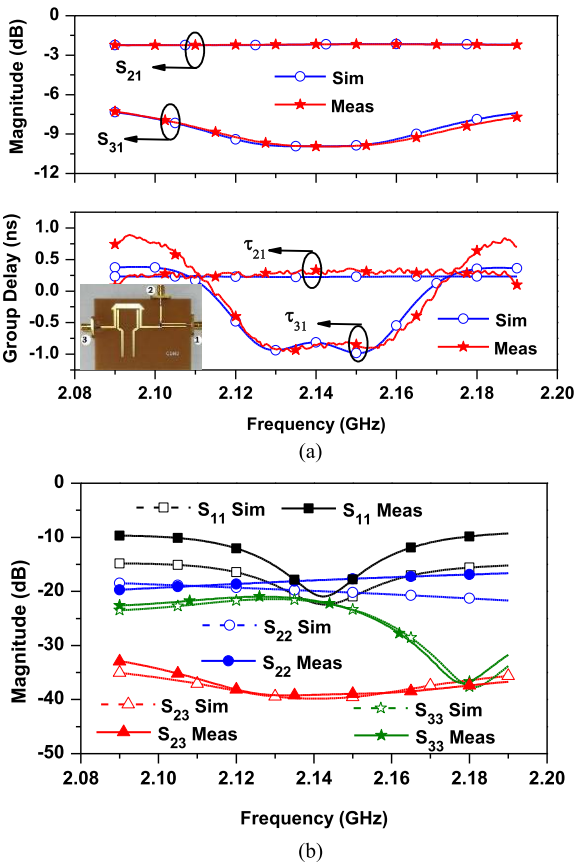

Fig. 11. Simulated and measured results for $k^2 = 0.6$. (a) Magnitude/GD. (b) Return losses/isolation characteristics.

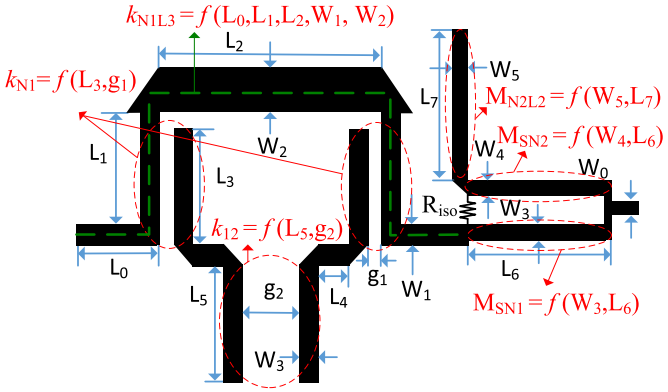

Fig. 12. EM-simulation layout of power divider with $k^2 = 1$. Physical dimensions: $L_0 = 15.8$, $L_1 = 12.2$, $L_2 = 18.1$, $L_3 = 14$, $L_4 = 1.5$, $L_5 = 20$, $L_6 = 19$, $L_7 = 19$, $W_0 = 1.5$, $W_1 = 1.8$, $W_2 = 3.70$, $W_3 = 0.76$, $W_4 = 0.76$, $W_5 = 1.5$, $g_1 = 0.5$, and $g_2 = 6.9$ (unit: mm).

Figs. 13 and 14 show the simulated and measured S-parameters and GDs through different transmission paths. From the measurement, the magnitudes of S-parameters are determined as $S_{21} = -3.21$ dB, $S_{31} = -8.701$ dB, $S_{11} = -19.92$ dB, $S_{22} = -18.26$ dB, $S_{33} = -17.79$ dB, and $S_{23} = -33.97$ dB at $f_0 = 2.14$ GHz. Similarly, the GDs of the transmission paths are obtained as $\tau_{21} = 0.3079$ ns and $\tau_{31} = -0.8281 \pm 0.11$ ns at $f_0 = 2.14$ GHz. The measured NGD

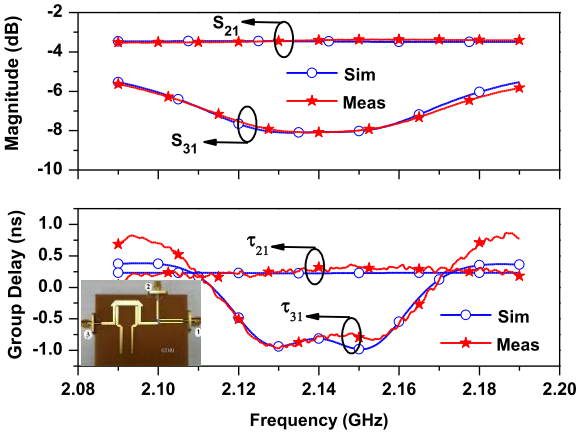

Fig. 13. Simulated and measured magnitude/GD characteristics for $k^2 = 1$.

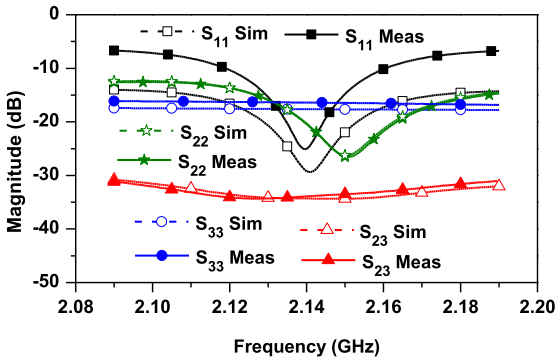

Fig. 14. Simulated and measured return losses/isolation characteristics for $k^2 = 1$.

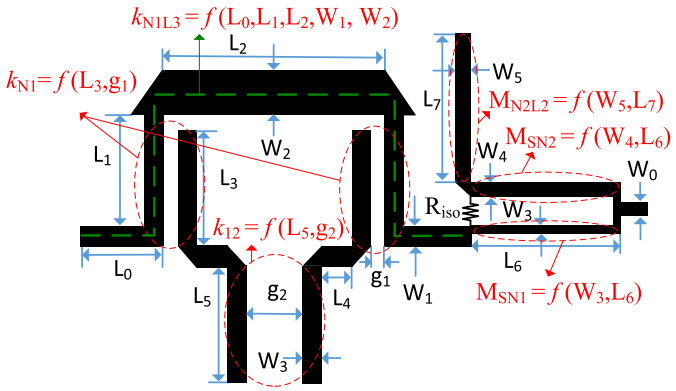

Fig. 15. EM-simulation layout of power divider with $k^2 = 2$. Physical dimensions: $L_0 = 15.8$, $L_1 = 12.2$, $L_2 = 18$, $L_3 = 14$, $L_4 = 1.5$, $L_5 = 20$, $L_6 = 19$, $L_7 = 19$, $W_0 = 1.5$, $W_1 = 1.8$, $W_2 = 3.70$, $W_3 = 0.5$, $W_4 = 1.86$, $W_5 = 2.4$, $g_1 = 0.5$, and $g_2 = 6.8$ (unit: mm).

bandwidth is given as 60 MHz. The return losses and isolation between the output ports are higher than 11.4 and 30.4 dB, respectively, in the overall measured bandwidth.

The EM-simulation layout and physical dimensions of the power divider with $k^2 = 2$ are shown in Fig. 15. The coupling parameters of the designed power divider are calculated as $M_{SN2} = 0.4082$, $M_{N2L2} = 0.7071$, $M_{SN1} = 0.8165$, $M_{N1} = 1.10$, $M_{12} = 1.210$, $M_{N1L3} = 1.4653$, $Q_u = 50$, and $\Delta = 2\%$.

The simulated and measured magnitudes and GDs are shown in Fig. 16. The measured magnitudes and GDs are determined as $S_{21} = -4.98$ dB, $S_{31} = -7.48$ dB,

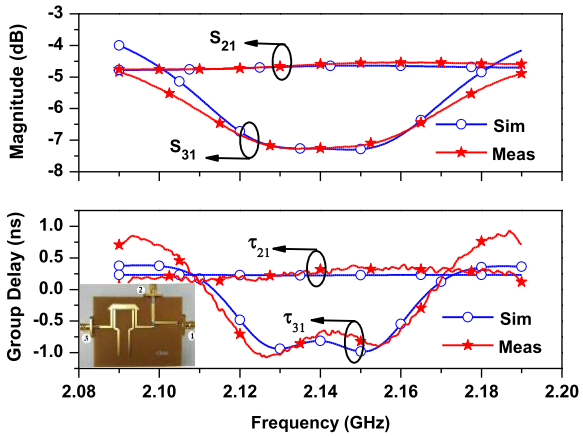

Fig. 16. Simulated and measured magnitude/GD for $k^2 = 2$.

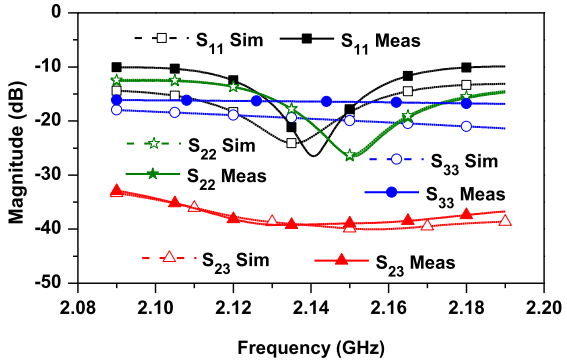

Fig. 17. Simulated and measured return losses/isolation characteristics for $k^2 = 2$.

TABLE II
S-PARAMETERS COMPARISON OF THE CONVENTIONAL AND THE PROPOSED POWER DIVIDERS

k^2	Conventional PD*		Measured Results of Proposed PD		
	S_{21c} (dB)	S_{31c} (dB)	S_{21p} (dB)	S_{31p} (dB)	S_{NGD} (dB)
0.6	-2.04	-4.26	-2.26	-9.96	-5.70
1	-3.01	-3.01	-3.21	-8.70	-5.69
2	-4.77	-1.76	-4.98	-7.48	-5.72

PD : Power divider
* : Ideal calculated results for conventional PD

$\tau_{21} = 0.3447$ ns, and $\tau_{31} = -0.8512 \pm 0.36$ ns at $f_0 = 2.141$ GHz. The measured NGD bandwidth is given as 60 MHz. Similarly, the simulated and measured return losses and isolation characteristics are shown in Fig. 17. The measured return losses and isolation are determined as $S_{11} = -20.86$ dB, $S_{22} = -17.46$ dB, $S_{33} = -19.73$ dB, and $S_{23} = -33.4$ dB at f_0.

The return losses and isolation characteristics are higher than 10.9 dB and 30.1 dB, respectively, in the overall measured bandwidth. Table II shows the S-parameters comparison of the conventional and the proposed dividers. As shown in Table II, the insertion losses of the proposed power divider between ports 3 and 1 are higher than that of the conventional because the NGD circuit loss is added on this path. The main advantage of the proposed power divider is to provide the NGD through ports 3 and 1 with some additional insertion loss.

IV. Conclusion

In this paper, we presented the GD analysis of the arbitrary power division ratio power divider using the coupling matrix approach. The proposed circuit does not require any lumped element to generate NGD; therefore, it provides fully distributed transmission line implementation. The proposed power divider provides positive and negative GDs through different transmission paths. Both theoretical and experimental results were provided for the verification of the proposed design method. The measurement results agreed well with the simulations and theoretical predicated values. The proposed circuit can be employed in feed networks of series-fed antenna arrays for minimizing the beam-squint problem and linear amplifiers for GD matching between different transmission paths.

References

[1] E. J. Wilkinson, "An N-way hybrid power divider," *IEEE Trans. Microw. Theory Techn.*, vol. MTT-8, no. 1, pp. 116–118, Jan. 1960.

[2] H. R. Ahn and I. Wolff, "General design equations, small-sized impedance transformers, and their applications to small-sized impedance transformers," *IEEE Trans. Microw. Theory Techn.*, vol. 49, no. 7, pp. 1277–1288, Jul. 2001.

[3] K. L. Wan, Y. L. Chow, and K. M. Luk, "Simple design of dual-frequency unequal power-divider," *Electron. Lett.*, vol. 37, no. 19, pp. 1171–1173, Sep. 2001.

[4] K. M. Cheng and P. Li, "A novel power-divider design with unequal power dividing ratio and simple layout," *IEEE Trans. Microw. Theory Techn.*, vol. 57, no. 6, pp. 1589–1594, Jun. 2009.

[5] M. K. Mandal and X. S. Sanyal, "Reduced-length rat-race coupler," *IEEE Trans. Microw. Theory Techn.*, vol. 55, no. 12, pp. 2593–2598, Dec. 2007.

[6] H. R. Ahn and S. Nam, "Wideband microstrip coupled-line ring hybrids for high power division rations," *IEEE Trans. Microw. Theory Techn.*, vol. 61, no. 5, pp. 1768–1780, May 2013.

[7] H.-R. Ahn, "Compact CVT-/CCT-unequal power dividers for high-power division ratios and design methods for arbitrary phase differences," *IEEE Trans. Microw. Theory Techn.*, vol. 62, no. 12, pp. 2954–2964, Dec. 2014.

[8] H.-R. Ahn, Y. Kim, and B. Kim, "Planar 10:1 Unequal three-port power dividers using general design equations," *Electron. Lett.*, vol. 48, no. 15, pp. 934–935, Jul. 2012.

[9] B. Li, X. Wu, and W. Wu, "A 10:1 Unequal Wilkinson power divider using coupled lines with two shorts," *IEEE Microw. Wireless Compon. Lett.*, vol. 19, no. 12, pp. 789–791, Dec. 2009.

[10] M.-C. J. Chik and K.-K. M. Cheng, "Group delay investigation of rat-race coupler design with tunable power dividing ratio," *IEEE Microw. Wireless Compon. Lett.*, vol. 24, no. 5, pp. 324–326, May 2014.

[11] J. Yi, Y. Yang, M. Park, W. Kang, and B. Kim, "Analog predistortion linearizer for high power RF amplifiers," *IEEE Trans. Microw. Theory Techn.*, vol. 48, no. 12, pp. 2709–2713, Dec. 2000.

[12] Y. Kim, I. S. Chang, and Y. Jeong, "An analog predistortion linearizer design," *Microw. J.*, vol. 48, no. 2, pp. 118–226, Feb. 2005.

[13] G. Chaudhary and Y. Jeong, "A design of power divider with negative group delay characteristics," *IEEE Microw. Wireless Compon. Lett.*, vol. 25, no. 6, pp. 394–396, Jun. 2015.

[14] S. Keser and M. Mojahedi, "Removal of beam squint in series fed array antennas using abnormal group delay phase shifters," in *Proc. Antennas Propag. Soc. Int. Symp. (APSURSI)*, Jul. 2010, pp. 1–4.

[15] H. Mirzaei and G. V. Eleftheriades, "Arbitrary-angle squint-free beamforming in series-fed antenna arrays using non-Foster elements synthesized by negative group delay networks," *IEEE Trans. Antennas Propag.*, vol. 63, no. 5, pp. 1997–2010, May 2015.

[16] S. S. Oh and L. Shafai, "Compensated circuit with characteristic of lossless double negative materials and its application to array antennas," *Microw., Antennas Propag.*, vol. 1, no. 1, pp. 29–38, Feb. 2007.

[17] W. Alomar and A. Mortazawi, "Elimination of beam squint in uniformly excited series fed antenna arrays using negative group delay circuits," in *Proc. Antennas Propag. Soc. Int. Symp. (APSURSI)*, Jul. 2012, pp. 1–2.

[18] A. Taslimi, W. Alomar, and A. Mortazawi, "Phase compensated serially fed array using the antenna as a part of negative group delay circuit," in *IEEE Int. Microw. Symp. Dig.*, May 2015, pp. 1–4.

[19] M. Kitano, T. Nakanishi, and K. Sugiyama, "Negative group delay and superluminal propagation: An electronic circuit approach," *IEEE J. Sel. Topics Quantum Electron.*, vol. 9, no. 1, pp. 43–51, Jan. 2003.

[20] M. Kandic and G. E. Bridges, "Limits of negative group delay phenomenon in linear causal media," *Prog. Electromagn. Res.*, vol. 134, pp. 227–246, 2013.

[21] H. Mirzaei and G. V. Eleftheriades, "Realizing non-Foster reactive elements using negative group delay networks," *IEEE Trans. Microw. Theory Techn.*, vol. 61, no. 12, pp. 4322–4332, Dec. 2013.

[22] H. Noto, K. Yamauchi, M. Nakayama, and Y. Isota, "Negative group delay circuit for feed-forward amplifier," in *IEEE Int. Microw. Symp. Dig.*, Jun. 2007, pp. 1103–1106.

[23] H. Choi, Y. Jeong, C. D. Kim, and J. S. Kenney, "Efficiency enhancement of feedforward amplifiers by employing a negative group delay circuit," *IEEE Trans. Microw. Theory Techn.*, vol. 58, no. 5, pp. 1116–1125, May 2010.

[24] H. Choi, Y. Jeong, C. D. Kim, and J. S. Kenney, "Bandwidth enhancement of an analog feedback amplifier by employing a negative group delay circuit," *Prog. Electromagn. Res.*, vol. 105, pp. 253–272, 2010.

[25] Y. Jeong, H. Choi, and C. D. Kim, "Experimental verification for time advancement of negative group delay in RF electronics circuits," *Electron. Lett.*, vol. 46, no. 4, pp. 306–307, Feb. 2010.

[26] S. Lucyszyn, I. D. Robertson, and A. H. Aghvami, "Negative group delay synthesizer," *Electron. Lett.*, vol. 29, no. 9, pp. 798–800, Apr. 1993.

[27] S. Lucyszyn and I. D. Robertson, "Analog reflection topology building blocks for adaptive microwave signal processing applications," *IEEE Trans. Microw. Theory Techn.*, vol. 43, no. 3, pp. 601–611, Mar. 1995.

[28] B. Ravelo, A. Pérennec, M. L. Roy, and Y. G. Boucher, "Active microwave circuit with negative group delay," *IEEE Microw. Wireless Compon. Lett.*, vol. 17, no. 12, pp. 861–863, Dec. 2007.

[29] M. Kandic and G. E. Bridges, "Asymptotic limit of negative group delay in active resonator-based distributed circuits," *IEEE Trans. Circuits Syst. I, Reg. Papers*, vol. 58, no. 8, pp. 1727–1735, Aug. 2011.

[30] C. D. Broomfield and J. K. A. Everard, "Broadband negative group delay networks for compensation of microwave oscillators and filters," *Electron. Lett.*, vol. 9, no. 23, pp. 1931–1932, Nov. 2000.

[31] O. F. Sidhiqui, M. Mojahedi, and G. V. Eleftheriades, "Periodically loaded transmission line with effective negative group delay index and negative group velocity," *IEEE Trans. Antennas Propag.*, vol. 51, no. 10, pp. 2619–2625, Oct. 2010.

[32] G. Chaudhary and Y. Jeong, "Distributed transmission line negative group delay circuit with improved signal attenuation," *IEEE Microw. Wireless Compon. Lett.*, vol. 24, no. 1, pp. 20–22, Jan. 2014.

[33] G. Chaudhary and Y. Jeong, "Transmission-line negative group delay networks with improved signal attenuation," *IEEE Antennas Wireless Propag. Lett.*, vol. 13, pp. 1039–1042, 2014.

[34] G. Chaudhary and Y. Jeong, "Low signal attenuation negative group delay network topologies using coupled lines," *IEEE Trans. Microw. Theory Techn.*, vol. 62, no. 10, pp. 2316–2324, Oct. 2014.

[35] G. Chaudhary, Y. Jeong, and J. Lim, "Microstrip line negative group delay filters for microwave circuits," *IEEE Trans. Microw. Theory Techn.*, vol. 62, no. 2, pp. 234–243, Feb. 2014.

[36] G. Chaudhary and Y. Jeong, "A design of compact wideband negative group delay network using cross coupling," *Microw. Opt. Technol. Lett.*, vol. 56, no. 11, pp. 2612–2616, Nov. 2014.

[37] C. T. M. Wu and I. Itoh, "Maximally flat negative group-delay circuit: A microwave transversal filter approach," *IEEE Trans. Microw. Theory Techn.*, vol. 62, no. 6, pp. 1330–1342, Jun. 2014.

[38] E. J. Naglich, J. Lee, D. Peroulis, and W. J. Chappell, "Switchless tunable bandstop to all-pass reconfigurable filter," *IEEE Trans. Microw. Theory Techn.*, vol. 60, no. 5, pp. 1258–1265, May 2012.

[39] J. Lee, E. J. Naglich, H. H. Sigmarsson, D. Peroulis, and W. J. Chappell, "New bandstop filter circuit topology and its application to design of a bandstop to bandpass switchable filter," *IEEE Trans. Microw. Theory Techn.*, vol. 61, no. 3, pp. 1114–1123, Mar. 2013.

[40] C. F. Chen, T. Y. Huang, T. M. Shen, and R. B. Wu, "Design of miniaturized filter power dividers for system-in-a package," *IEEE Trans. Compon., Packag., Manuf. Technol.*, vol. 3, no. 10, pp. 1663–1672, Oct. 2013.

[41] Y. Wu and Y. Liu, "A unequal coupled-line Wilkinson power divider for arbitrary terminated impedances," *Prog. Electromagn. Res.*, vol. 117, pp. 181–194, 2011.

Girdhari Chaudhary (S'10–M'13) received the B.E. degree in electronics and communication engineering from Nepal Engineering College, Kathmandu, Nepal, in 2004, the M.Tech. degree in electronics and communication engineering from MNIT, Jaipur, India, in 2007, and the Ph.D. degree in electronics engineering from Chonbuk National University, Jeonju, South Korea, in 2013.

He is currently an Assistant Research Professor with the Division of Electronics Engineering, Chonbuk National University. He was a Principal Investigator of independent project through the Basic Science Research Program of the National Research Foundation of Korea (NRF) funded by the Ministry of Education Korea. His current research interests include multiband tunable passive circuits, negative group delay circuits and its applications, and in-band full duplex systems and high-efficiency power amplifiers.

Dr. Chaudhary received the BK21 PLUS Research Excellence Award 2015 from the Ministry of Education, South Korea, and the Korean Research Fellowship from NRF funded by the Ministry of Science, ICT and Future Planning.

Yongchae Jeong (M'99–SM'10) received the B.S.E.E., M.S.E.E, and Ph.D. degrees in electronics engineering from Sogang University, Seoul, South Korea, in 1989, 1991, and 1996, respectively.

From 1991 to 1998, he was a Senior Engineer with Samsung Electronics, South Korea. From 2006 to 2007, he was a Visiting Professor with the Georgia Institute of Technology, Atlanta, GA, USA. Since 1998, he has been with the Division of Electronics Engineering, Chonbuk National University, Jeonju, South Korea, where he is currently a Professor, a Member of the IT Convergence Research Center, and the Director of the HOPE-IT Human Resource Development Center of BK21 PLUS. He is currently teaching and conducting research in the area of microwave passive and active circuits, mobile and satellite base-station RF system, the design of periodic defected transmission line, negative group delay circuits and its applications, and in-band full duplex radio and RFIC design. He has authored or coauthored over 170 papers in international journals and conference proceedings.

Prof. Jeong is a member of the Korea Institute of Electromagnetic Engineering and Science.